

NUMERICAL SIMULATION OF HYDRODYNAMIC AND HEAT-MASS EXCHANGE PROCESSES OF A MICROCLIMATE CONTROL SYSTEM IN AN INDUSTRIAL GREENHOUSE

Viktor TROKHANIAK¹ Oleksandra KLENDII²

Abstract: *Based on the conducted analysis, the main disadvantages of numerical simulation for greenhouses have been determined. Numerical simulation of hydrodynamic and heat-mass exchange processes, which take place when heating and ventilating systems interact inside operational buildings of industrial greenhouses, has been conducted. Having used ANSYS Fluent software package for numerical simulation, temperature and velocity fields, velocity vectors and radiant heat flows in a greenhouse have been obtained. The findings can be used in order to improve heating and ventilating systems of greenhouse complexes.*

Keywords: *numerical simulation, industrial greenhouse, heating and ventilating system, finite element method.*

1. Introduction

Growth and development of plants is closely connected with environmental conditions. The ability to create the conditions, which meet the requirements of plants, is a key to high yields. A set of necessary conditions, namely physical parameters of air and root zone environment in covered soil buildings, is called a microclimate. It is created by cooperative activity of the main systems of process equipment, namely they are heating, ventilating, irrigation, feed, carbon

dioxide nutrition and artificial lighting systems [5].

Every species of vegetable crops and even a separate cultivar species has its own optimum, maximum and minimum temperature. That is why one of the most important factors of managing plants growth and fructification is the creation of necessary temperature and humidity conditions, which are provided by heating and ventilating system activity [9].

Temperature and humidity conditions of a greenhouse are established as a result of heat and mass exchange processes, which take place indoor as well as through its

¹ National University of life and environmental sciences of Ukraine, Heroiv Oborony Str., 15, Kiev, Ukraine;

² Separated Subdivision of National University of Life and Environmental Sciences of Ukraine Berezahny Agrotechnical Institute, Akademichna Str., 20, Berezahny, Ukraine;

Correspondence: Viktor Trokhaniak; email: trohaniak.v@gmail.com.

outer walls made of single-layer polycarbonate.

Papers [10, 12-13] present the peculiarities of a three-dimensional temperature zone in a greenhouse. Based on the created mathematical model, a model of space-distributed temperature parameters of a greenhouse atmosphere has been simulated. In this case, parameter identification for each zone of a greenhouse section is conducted taking into consideration environmental pollution. The calculation and the experimental temperature values have been compared. The disadvantage of the simulation, which is suggested in the above mentioned papers, is the division of the building into sections. Calculation results for each section are transferred to the next zone, which can cause quite poor accuracy during a simulation process.

Computer-generated simulation and CFD analysis of air flow on the surface of greenhouses, which are located on roofs is aimed at the determination of forces and moments that influence them, forces and moments, which are caused by wind action as well as visualization of air, that flows on their outer surfaces [2-3]. For this purpose, ANSYS Fluent software is used, which is based on finite element method

[11]. Paper [4] presents experimental results on aerodynamic draft force and overall coefficients of resistance force of five greenhouse models under the influence of wind.

In addition, papers [7] show the results of numerical simulation using ANSYS Fluent and the results of experimental investigation [8] in 3D for aviaries.

2. Material and Method

The purpose of the work is to conduct computer-generated mathematical simulation of the processes of hydrodynamics and heat-mass exchange, which take place when heating and ventilating system interacts, in order to find out optimum temperature and humidity conditions.

Industrial greenhouse geometry (Figure 1, a.) was built according to its real size, that is why, there is a large number of elements and sides. Having taken this aspect into consideration, it was decided to calculate only one fourth of 3D greenhouse (Figure 1, b.), which is symmetrical to the other three and it was possible to save time for computer calculation.

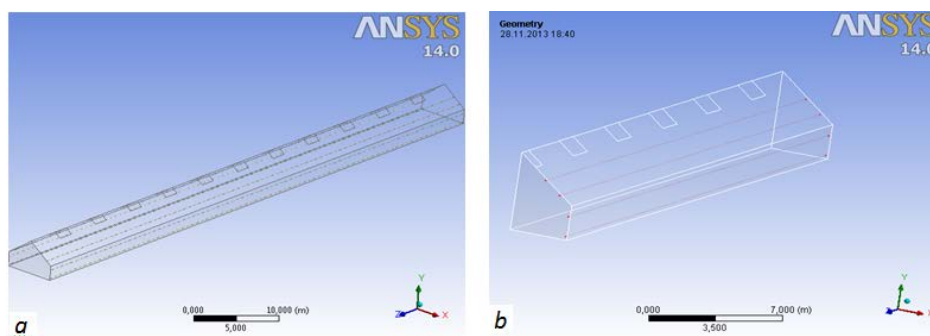


Fig. 1. General view of the geometry of a 3D greenhouse:
a – full size; b – symmetrical part of a greenhouse

The geometry of a greenhouse includes openings for an air ventilation system and pipes with hot water supply for heating.

Water temperature in a heating system is equal to $+95\dots+70^{\circ}\text{C}$ in case of heating supply from its own boiler plant. The inside temperature of a greenhouse is assumed to be $+15^{\circ}\text{C}$. External air temperature is assumed to be the average temperature of the coldest months of operation -20°C (the same as for a heated greenhouse). Relative humidity in a greenhouse is assumed to be 60%. Steel smooth pipes with the diameter of 32 mm and total surface area being 657.9 m^2 are used for heating a greenhouse. Greenhouse walls are made of single-layer cellular polycarbonate, which is 4 mm in thickness. The width and the length of a greenhouse section is 6.4 m and 75 m respectively and its height is 4.5 m.

When performing numerical calculation in order to solve tasks in hydrodynamics and heat-mass transfer, a finite element method is used. Mesh generation was conducted in ANSYS Meshing based on Workbench framework. In the process of mesh generation for a greenhouse, local mesh control method was used.

Figure 2 presents a generated mesh of an operational building of a greenhouse in section, with openings for air supply and hot water pipes for heating. The mesh is reduced to some extent in the places, where there are openings and pipes, relative to the rest of the building area. This is aimed at improving hydrodynamics and heat-mass exchange effects.

Figure 3 presents an enlarged view of a hot water pipe section, which makes it possible to see boundary layers clearly. There are two layers inside the pipe and two layers outside it.

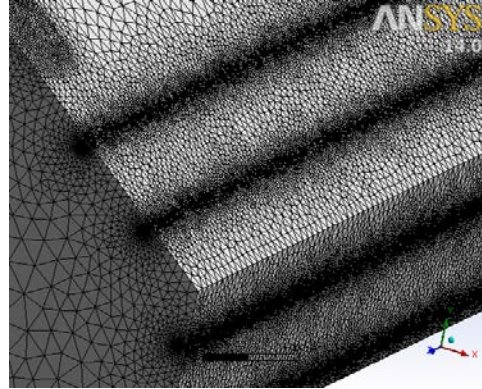


Fig. 2. General view of a greenhouse mesh in section with openings for air supply and pipes for water heating

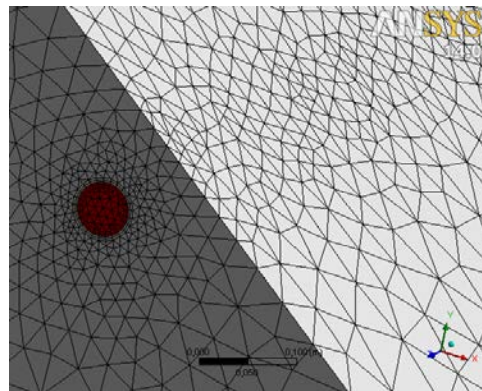


Fig. 3. A greenhouse mesh and a detailed view of a pipe for heating with its boundary layers

It is time consuming to choose the parameters of mesh generation settings in ANSYS Meshing in order to transfer calculations of heat-mass exchange and hydrodynamics to Ansys Fluent. Results accuracy of numerical simulation depends on a mesh quality indicator Orthogonal Quality [20].

Numerical mathematical simulation of hydrodynamic and heat-mass exchange processes in an industrial greenhouse was conducted. For this purpose, computer-generated simulation method based on ANSYS Fluent software was used. Navier-

Stokes equations [17] and energy-transfer equations for convective currents are the basis for this mathematical model. Spalarta-Allmarasa turbulence model [18-19] and Discrete Ordinates (DO) radiation model [1] were used for the calculations.

The computation was conducted using heating and ventilating systems in buildings during winter time, taking into account solar radiation.

Navier-Stokes equation has the form:

$$\left. \begin{aligned} \rho \left(\frac{\partial u}{\partial t} + u \frac{\partial u}{\partial x} + v \frac{\partial u}{\partial y} + w \frac{\partial u}{\partial z} \right) &= -\frac{\partial p}{\partial x} + \mu \left(\frac{\partial^2 u}{\partial x^2} + \frac{\partial^2 u}{\partial y^2} + \frac{\partial^2 u}{\partial z^2} \right), \\ \rho \left(\frac{\partial u}{\partial t} + u \frac{\partial u}{\partial x} + v \frac{\partial u}{\partial y} + w \frac{\partial u}{\partial z} \right) &= -\frac{\partial p}{\partial y} + \mu \left(\frac{\partial^2 u}{\partial x^2} + \frac{\partial^2 u}{\partial y^2} + \frac{\partial^2 u}{\partial z^2} \right), \\ \rho \left(\frac{\partial u}{\partial t} + u \frac{\partial u}{\partial x} + v \frac{\partial u}{\partial y} + w \frac{\partial u}{\partial z} \right) &= -\frac{\partial p}{\partial z} + \mu \left(\frac{\partial^2 u}{\partial x^2} + \frac{\partial^2 u}{\partial y^2} + \frac{\partial^2 u}{\partial z^2} \right), \end{aligned} \right\} \quad (1)$$

where:

ρ is medium density, kg/m³;
 μ – medium dynamic viscosity, Pa•s;
 p - pressure, Pa;
 u, v, w - velocity field of vectors;
 t - time, s.

A continuity equation has the form

$$\frac{\partial u}{\partial x} + \frac{\partial v}{\partial y} + \frac{\partial w}{\partial z} = 0. \quad (2)$$

An energy-conservation equation:

$$\rho C_p \left(V_x \frac{\partial T}{\partial x} + V_y \frac{\partial T}{\partial y} + V_z \frac{\partial T}{\partial z} \right) = \frac{\partial}{\partial x} \left(\lambda \frac{\partial T}{\partial x} \right) + \frac{\partial}{\partial y} \left(\lambda \frac{\partial T}{\partial y} \right) + \frac{\partial}{\partial z} \left(\lambda \frac{\partial T}{\partial z} \right), \quad (3)$$

where:

T is point temperature, °K;
 λ – coefficient of medium heat transfer capacity, W/m•°K;
 C_p – specific heat capacity of a medium, J/kg•°K.

And boundary conditions (Figure 4, a.) in the middle of the room of greenhouse along the yOx plane:

$$\left. \frac{\partial T}{\partial x} \right|_{x=M/2=0} \quad \text{and} \quad \left. \frac{\partial W}{\partial x} \right|_{z=M/2=0}. \quad (5)$$

Boundary Conditions

Let us set boundary conditions (Figure 4, b.) in the middle of the room of greenhouse along the yOz plane:

$$\left. \frac{\partial T}{\partial z} \right|_{z=L/2=0} \quad \text{and} \quad \left. \frac{\partial W}{\partial z} \right|_{z=L/2=0}. \quad (4)$$

The boundary conditions of the third kind on the side wall of greenhouse have the form:

$$\begin{aligned} 0 &\leq y \leq H; \\ x &= M/2; \\ 0 &\leq z \leq L/2; \\ -\lambda_w \left. \frac{\partial T_w}{\partial x} \right|_{x=M/2} &= \alpha (T_w - T_{en}). \end{aligned} \quad (6)$$

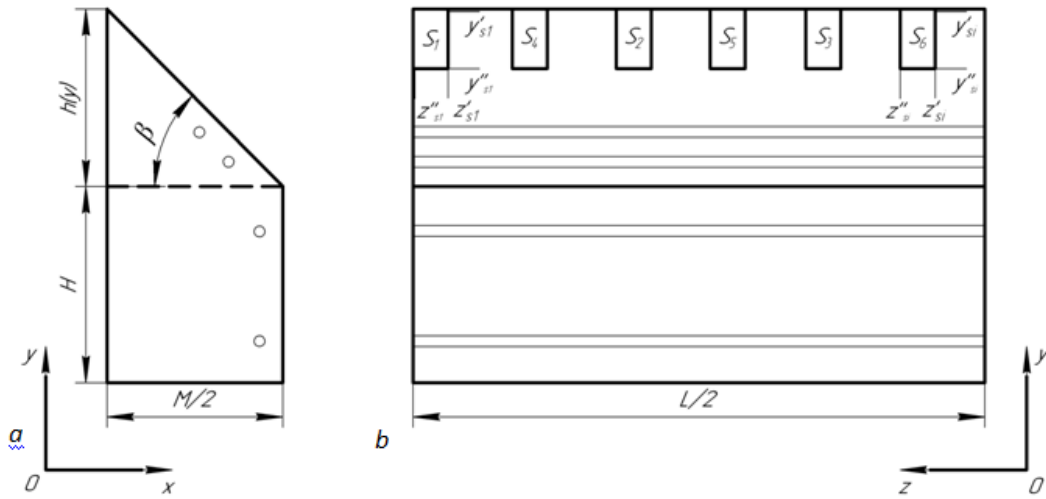


Fig. 4. General view of the projection of the walls of the greenhouse:
 a – the side wall; b – the end wall

Attachment conjugation on the side wall of greenhouse:

$$T_h(x = M/2) = T_w(x = M/2);$$

$$\lambda_h \frac{\partial T_h}{\partial x} \Big|_{x=M/2} = \lambda_w \frac{\partial T_w}{\partial x} \Big|_{x=M/2}. \quad (7)$$

Attachment conjugation on the end wall of greenhouse:

$$T_h(z = 0) = T_w(z = 0);$$

$$\lambda_h \frac{\partial T_h}{\partial z} \Big|_{z=0} = \lambda_w \frac{\partial T_w}{\partial z} \Big|_{z=0}. \quad (10)$$

Attachment conditions on the side wall:

$$W_w(x = M/2) = 0. \quad (8)$$

Attachment conditions on the end wall:

$$W_w(z = 0) = 0. \quad (11)$$

Boundary conditions of the third kind on the end wall:

$$0 \leq x \leq M/2;$$

$$0 \leq y \leq H + h - x / \cos \beta;$$

$$z = 0;$$

$$-\lambda_w \frac{\partial T_{CT}}{\partial z} \Big|_{z=0} = \alpha (T_w - T_{en}). \quad (9)$$

Boundary conditions of the third kind on the roof surface of greenhouse:

$$0 \leq x \leq M/2;$$

$$0 \leq y \leq H + h - x / \cos \beta;$$

$$0 \leq z \leq L/2;$$

$$-\lambda_w \frac{\partial T_{CT}}{\partial z} \Big|_{\substack{S_x = x / \cos \beta \\ S_y = H + y / \sin \beta}} =$$

$$= \alpha \left(T_w \Big|_{\substack{S_x = x / \cos \beta \\ S_x = H + y / \sin \beta}} - T_{Ln} \right). \quad (12)$$

Attachment conjugation on the roof surface:

$$T_h \begin{pmatrix} S_x = x / \cos \beta \\ S_y = H + y / \sin \beta \end{pmatrix} = T_w \begin{pmatrix} S_x = x / \cos \beta \\ S_y = H + y / \sin \beta \end{pmatrix} \quad (13)$$

$$\lambda_h \frac{\partial T_h}{\partial n} \Big|_{S_x = x / \cos \beta, S_y = H + y / \sin \beta} = \lambda_w \frac{\partial T_w}{\partial n} \Big|_{S_x = x / \cos \beta, S_y = H + y / \sin \beta}$$

Attachment conditions on the roof surface:

$$W_w \begin{pmatrix} S_x = x / \cos \beta \\ S_y = H + y / \sin \beta \end{pmatrix} = 0. \quad (14)$$

The boundary conditions for ventilation openings on the roof surface:

$$\begin{aligned} x'_{s_i} &\leq x \leq x''_{s_i} \\ S_i(x_{s_i} = x / \cos \beta); \\ y'_{s_i} &\leq y \leq y''_{s_i}; \\ S_i(y_{s_i} = H + y / \sin \beta); \\ z'_{s_i} &\leq z \leq z''_{s_i}; \\ S_i(z_{s_i} = z_i + z); \\ i &= 1, 2, 3; \\ W &= W_{in}; \\ T &= T_{en}. \end{aligned} \quad (15)$$

The boundary conditions for ventilation openings on the roof surface:

$$\begin{aligned} x'_{s_i} &\leq x \leq x''_{s_i} \\ S_i(x_{s_i} = x / \cos \beta); \\ y'_{s_i} &\leq y \leq y''_{s_i}; \\ S_i(y_{s_i} = H + y / \sin \beta); \\ z'_{s_i} &\leq z \leq z''_{s_i}; \\ S_i(z_{s_i} = z_i + z); \\ i &= 4, 5, 6; \\ W &= W_{out}; \\ T &= T_h. \end{aligned} \quad (16)$$

Attachment conjugation on the surface of heating pipes:

$$\begin{aligned} T_h(x = x_w) &= T_w(x = x_w); \\ T_h(y = y_w) &= T_w(y = y_w); \\ \lambda_h \frac{\partial T_h}{\partial n} \Big|_{x=x_w} &= \lambda_w \frac{\partial T_w}{\partial n} \Big|_{x=x_w}; \\ \lambda_h \frac{\partial T_h}{\partial n} \Big|_{y=y_w} &= \lambda_w \frac{\partial T_w}{\partial n} \Big|_{y=y_w}. \end{aligned} \quad (17)$$

Attachment conditions on the surface of heating pipes:

$$x = x_w; \quad y = y_w; \quad W = 0. \quad (18)$$

where:

- L is the length of greenhouse sidewalls, m;
- M – the width of the front and the back end wall, m;
- H – the height of the greenhouse, m;
- $h(y)$ – the function of roof wall height in section Oy , m;
- T_w – wall temperature, °C;
- T_{en} – environment temperature, °C;
- W_{in} – inlet air velocity when entering the greenhouse, m/s;
- W_{out} – outlet air velocity when leaving the greenhouse, m/s;
- W_w – air velocity at the wall, m/s;
- α – coefficient of the heat transfer, $W/m^2 \cdot ^\circ K$;
- λ_h – coefficient of heat transfer capacity of a coolant, $W/m \cdot ^\circ K$;
- λ_w – coefficient of heat transfer capacity of a wall, $W/m \cdot ^\circ K$;
- T_h – temperature of a coolant, °C;
- β – angle of inclination of the surface of the roof, grad;
- n – normal to the surface of the roof;
- S_x – the value of the roof projection plane the Ox axis, m;
- S_y – the value of the roof projection plane the Oy axis, m.

Spalarta-Allmarasa turbulence model

The transported variable in the Spalart-Allmaras model, $\tilde{\nu}$, is identical to the turbulent kinematic viscosity except in the

near-wall (viscosity-affected) region. The transport equation for the modified turbulent viscosity $\tilde{\nu}$ is:

$$\frac{\partial}{\partial t}(\rho\tilde{\nu}) + \frac{\partial}{\partial x_i}(\rho\tilde{\nu}u_i) = G_\nu + \frac{1}{\sigma_{\tilde{\nu}}} \left[\frac{\partial}{\partial x_i} \left\{ (\mu + \rho\tilde{\nu}) \frac{\partial \tilde{\nu}}{\partial x_i} \right\} + C_{b2\rho} \left(\frac{\partial \tilde{\nu}}{\partial x_i} \right)^2 \right] - Y_\nu + S_{\tilde{\nu}}, \quad (19)$$

where G_ν is the production of turbulent viscosity, and Y_ν is the destruction of turbulent viscosity that occurs in the near-wall region due to wall blocking and viscous damping. $\sigma_{\tilde{\nu}}$ and C_{b2} are the constants and ν is the molecular kinematic viscosity. $S_{\tilde{\nu}}$ is a user-defined source term.

Discrete Ordinates (DO) radiation model

The radiative transfer equation for an absorbing, emitting, and scattering medium at position \vec{r} in the direction \vec{s} is:

$$\frac{dI(\vec{r}, \vec{s})}{ds} + (\alpha + \sigma_s)I(\vec{r}, \vec{s}) = \alpha n^2 \frac{\sigma T^4}{\pi} + \frac{\sigma_s}{4\pi} \int_0^{4\pi} I(\vec{r}, \vec{s}') \Phi(\vec{s} \cdot \vec{s}') d\Omega', \quad (20)$$

where:

- \vec{r} is position vector;
- \vec{s} – direction vector;
- \vec{s}' – scattering direction vector;
- s – path length;
- α – absorption coefficient;
- n – refractive index;
- σ_s – scattering coefficient;
- σ – Stefan-Boltzmann constant ($5,669 \cdot 10^{-8} \text{ W/m}^2 \cdot \text{K}^4$);
- I – radiation intensity, which depends on position (\vec{r}) and direction (\vec{s});
- Φ – phase function;
- Ω' – solid angle; $(\alpha + \sigma_s)s$ is the optical thickness or opacity of the medium.

model solves the radiative transfer equation (RTE) for a finite number of discrete solid angles, each associated with a vector direction fixed in the global Cartesian system (x, y, z). The uncoupled implementation is sequential in nature and uses a conservative variant of the DO model called the finite-volume scheme [6, 16], and its extension to unstructured meshes [15]. In the uncoupled case, the equations for the energy and radiation intensities are solved one by one, assuming prevailing values for other variables.

The refractive index n is important when considering radiation in semi-transparent media. The discrete ordinates radiation

The discrete ordinates model considers the radiative transfer equation in the direction \vec{s} as a field equation. Thus, equation (20) is written as:

$$\nabla \cdot (I(\vec{r}, \vec{s})\vec{s}) + (\alpha + \sigma_s)I(\vec{r}, \vec{s}) = \alpha n^2 \frac{\sigma T^4}{\pi} + \frac{\sigma_s}{4\pi} \int_0^{4\pi} I(\vec{r}, \vec{s}') \Phi(\vec{s} \cdot \vec{s}') d\Omega' \quad (21)$$

ANSYS Fluent also allows the modeling of non-gray radiation using a gray-band model.

The RTE for the spectral intensity $I_\lambda(\vec{r}, \vec{s})$ can be written as [20]:

$$\nabla \cdot (I_\lambda(\vec{r}, \vec{s})\vec{s}) + (a_\lambda + \sigma_s)I_\lambda(\vec{r}, \vec{s}) = a_\lambda I_{b\lambda} + \frac{\sigma_s}{4\pi} \int_0^{4\pi} I_\lambda(\vec{r}, \vec{s}') \phi(\vec{s} \cdot \vec{s}') d\Omega'. \quad (22)$$

Here λ is the wavelength, a_λ is the spectral absorption coefficient, and $I_{b\lambda}$ is the black body intensity given by the Planck function. The scattering coefficient, the scattering phase function, and the refractive index n are assumed independent of wavelength.

The non-gray DO implementation divides the radiation spectrum into N wavelength bands, which need not be contiguous or equal in extent. The wavelength intervals are supplied by you, and correspond to values in vacuum ($n=1$). The RTE is integrated over each wavelength interval, resulting in transport equations for the quantity $I_\lambda \Delta\lambda$, the radiant energy contained in the wavelength band $\Delta\lambda$. The behavior in each band is assumed gray. The black body emission in the wavelength band per unit solid angle is written as

$$[F(0 \rightarrow n\lambda_2 T) - F(0 \rightarrow n\lambda_1 T)] n^2 \frac{\sigma T^4}{\pi}, \quad (23)$$

where $F(0 \rightarrow n\lambda T)$ is the fraction of radiant energy emitted by a black body [14] in the wavelength interval from 0 to λ at temperature T in a medium of refractive index n . λ_2 and λ_1 are the wavelength boundaries of the band.

The total intensity $I(\vec{r}, \vec{s})$ in each direction \vec{s} at position \vec{r} is computed using:

$$I(\vec{r}, \vec{s}) = \sum_k I_{\lambda_k}(\vec{r}, \vec{s}) \Delta\lambda_k, \quad (24)$$

where the summation is over the wavelength bands.

Boundary conditions for the non-gray DO model are applied on a band basis. The treatment within a band is the same as that for the gray DO model.

3. Results and Discussions

Calculation results of numerical simulation for an industrial greenhouse are represented in Figures 5 - 12. Figures 5–7 show temperature fields in an operational section of a greenhouse in various sectional views.

Figure 7 represents the overall view of the surface of a greenhouse operational section, where there are temperature fluctuations ranging from 272 °K to 295 °K (from -1.15 °C to +21.85 °C). In the lower area, which is closer to the floor, the temperature is quite elevated. Figure 6 shows the cross section of a heating pipe with heat carrying medium in a greenhouse.

Air velocity vectors are represented in Figure 8, and air temperature fields – in Figure 8, b. These data show that air velocity near a heating pipe varies within the range of 0.1-0.4 m/s and an average temperature of a heat carrying medium is 355 °K (+81.85 °C). Figures 9 - 11 present simulation results for air velocity in a greenhouse production

section in various sections, which show that the maximum air velocity is 1.65 m/s.

Figure 9 shows air velocity fields (Figure 9, a.) and air velocity vectors (Figure 9, b.) in a greenhouse in cross section along Oy axis in the middle of the inlet section of a

ventilation opening. The maximum speed is concentrated in the middle of a greenhouse and reaches 1.52 m/s at certain points.

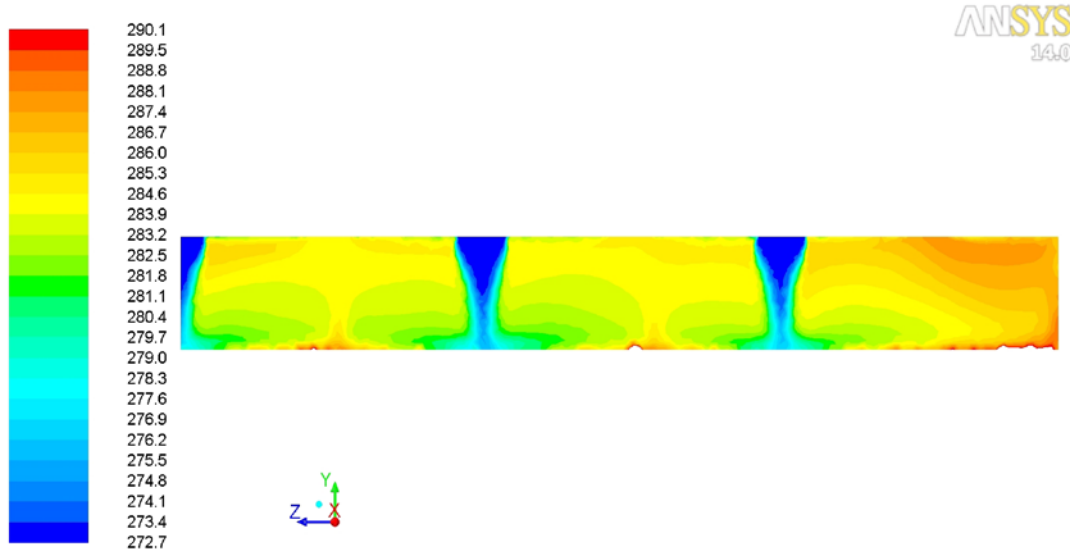


Fig. 5. The change of temperature fields in longitudinal section along the median line of the symmetrical half of a greenhouse section, °K

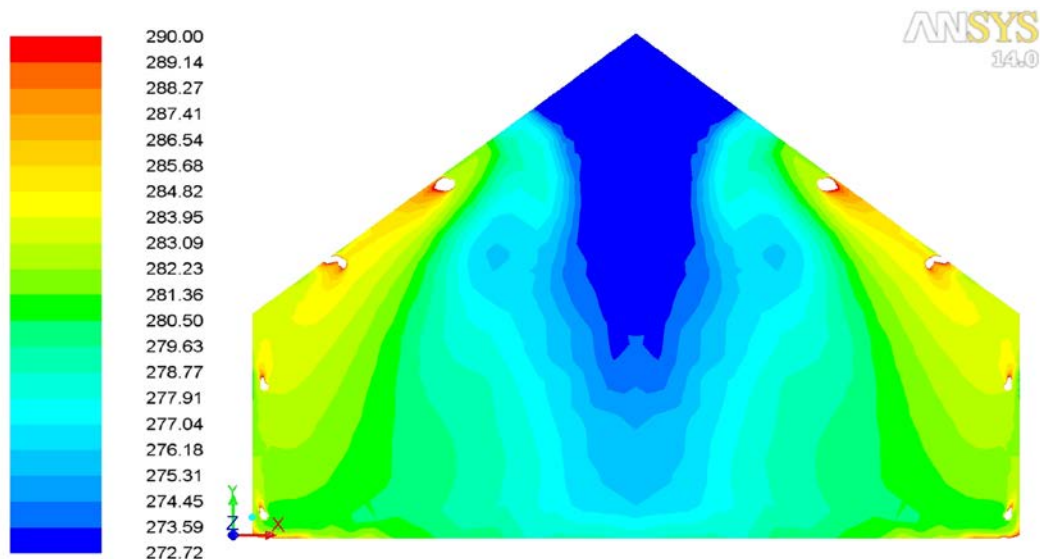


Fig. 6. The change of temperature fields in a greenhouse in cross section along Oy axis in the middle of an air inlet

Air velocity vectors in longitudinal section of a greenhouse part in the middle of the building are represented in Fig. 10. Vectors concentration is observed in the places, where air is supplied to a greenhouse and where air leaves a greenhouse through ventilation openings (ventilators).

The maximum air velocity of 1.6 m/s is reached after it passes through ventilators and gets inside a greenhouse, but when

air reaches the lower area of a building (soil), its speed decreases rapidly and its average value is ranging from 0.4 m/s to 0.5 m/s.

The above mentioned air velocity in a greenhouse does not exceed the optimum rate (0.3...0.5 m/s), and it can be increased in the above plants area up to 1...1.5 m/s in order to improve air circulation conditions around plant leaves in a greenhouse [5].

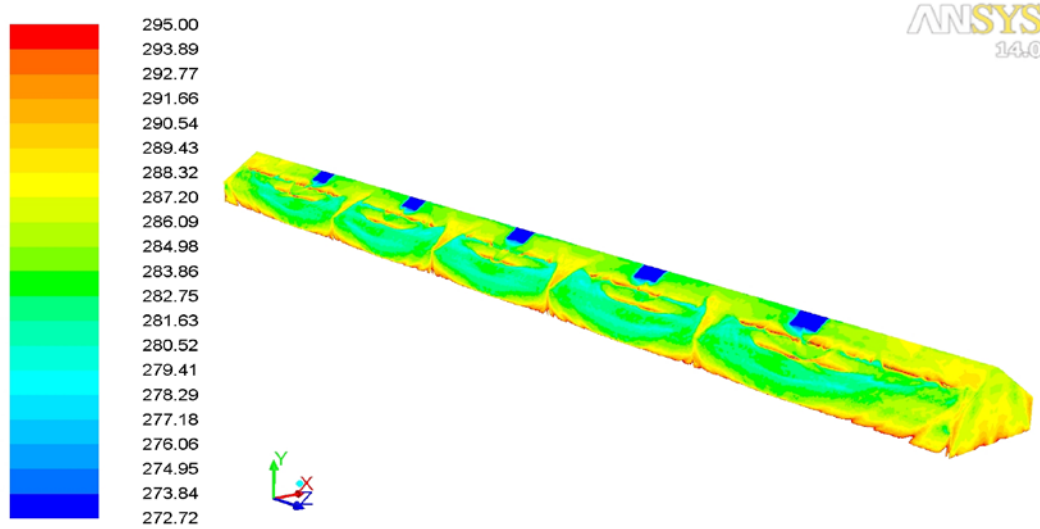


Fig. 7. *Temperature fields in the overall view of a greenhouse section*

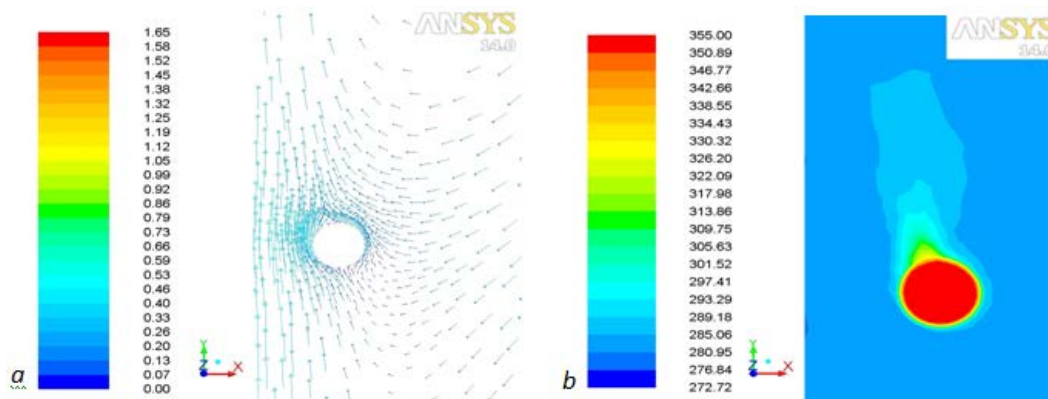


Fig. 8. *Cross section of a heating pipe with heat carrying medium in a greenhouse: a – air velocity vectors, m/s; b – air temperature fields, °K*

Figure 12 shows radiation thermal fields in the overall view of a greenhouse section.

It can be seen, that radiation heat flow density reaches the value of 37 W/m^2 .

As a result of numerical simulation of hydrodynamic and heat-mass exchange

processes, that take place when heating and ventilating systems interact, the analysis of temperature distribution, radiation heat flows and air velocity in an operational section of a greenhouse was conducted.

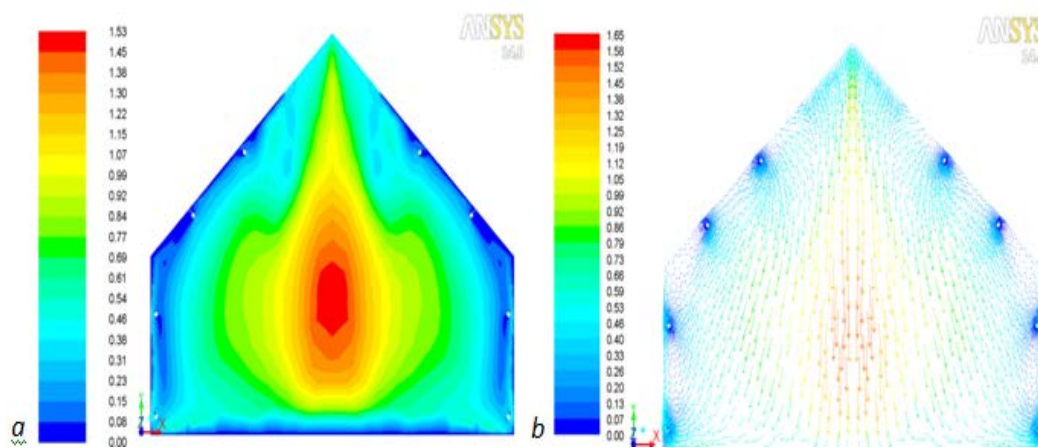


Fig. 9. The change of air velocity in a greenhouse in cross section along Oy axis in the middle of a ventilation opening, m/s: a – velocity fields; b – velocity vectors

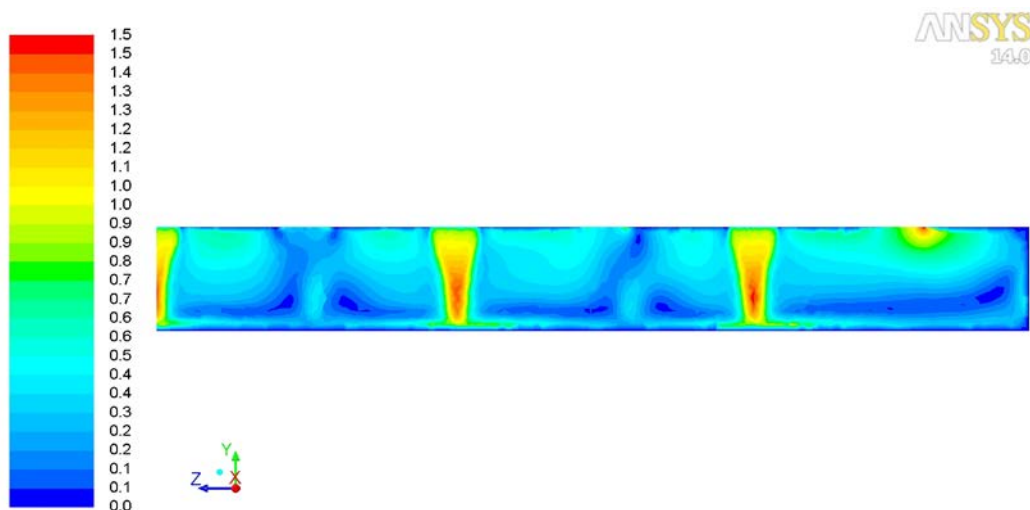


Fig. 10. Air velocity field in longitudinal section along the median line of the symmetrical half of a greenhouse section, m/s

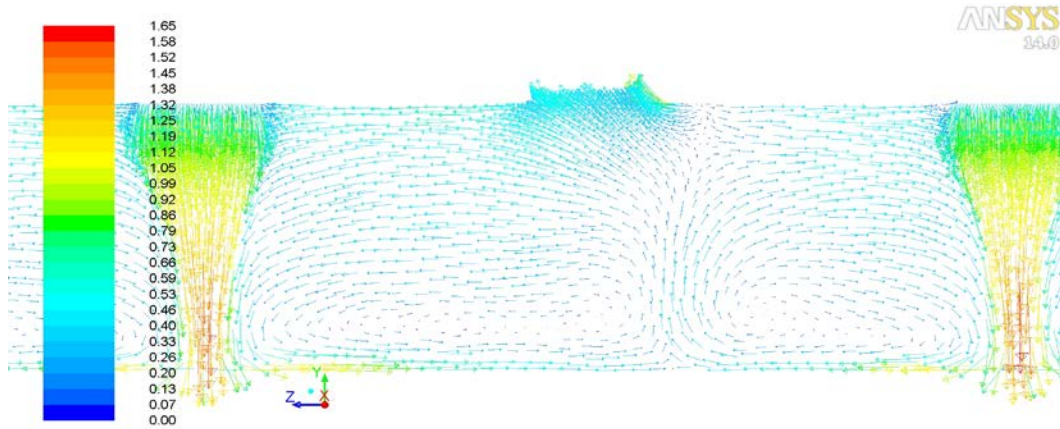


Fig. 11. Air velocity vectors in longitudinal section along the median line of a greenhouse section, m/s

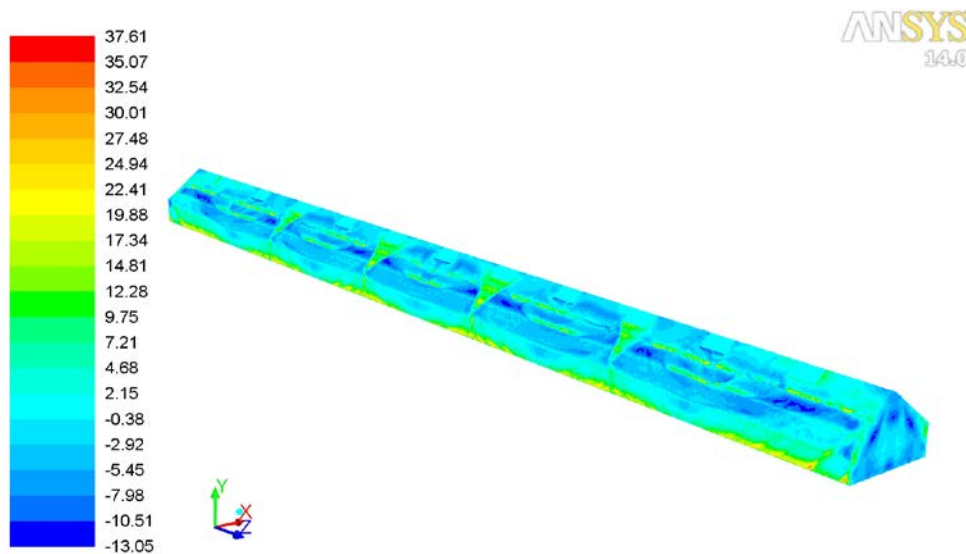


Fig. 12. Radiation heat fields in the overall view of a greenhouse section, W/m^2

4. Conclusions

Having used ANSYS Fluent software, computer-generated mathematical simulation of hydrodynamic and heat-mass exchange processes inside a greenhouse building, which take place when heating and ventilating systems interact, have been conducted.

The analysis of velocity vectors, temperature fields and radiation heat flows, which were obtained from numerical simulation, has been conducted.

The data, necessary to assess and create the optimum temperature and humidity conditions in operational buildings of an

industrial greenhouse, have been obtained.

References

1. ANSYS, 2011. ANSYS Fluent Theory Guide. Release. Published in the U.S.A, 794 p.
2. Badiu, E.C., Bratucu, Gh., 2014. The Effects of Wind on Roof Systems for Buildings. In: Bulletin of the Transilvania University of Brasov, Series II, vol. 7(56), no. 1, pp. 67-72.
3. Badiu, E.C., Lateş, M.T., Bratucu, Gh., 2015. The simulation of the solicitations to which greenhouses located on rooftops are subjected based on modelling with the finite element method. In: Bulletin of the Transilvania University of Brasov, Series II, vol. 8(57), no. 2, pp. 61-68.
4. Badiu, E.C., Lateş, M.T., Bratucu, Gh.C., 2016. Experimental research on determination of drag coefficient of the greenhouses located on roofs of buildings. In: Bulletin of the Transilvania University of Brasov, Series II, vol. 9(58), no. 1, pp. 43-50.
5. Belohubova, Y.N., Vasilyev, A.M., Gyl, L.S. et al., 2006. Modern Vegetable Growing in the Open and Protected Horticulture. In: OAO "Publishing House "Kyiv. Pravda", 528 p.
6. Chui, E.H., Raithby, G.D., 2013. Computation of radiant heat transfer on a non-orthogonal mesh using the finite-volume method. In: Numerical Heat Transfer, vol. 23, part B, pp. 269-288.
7. Gorobets, V.G., Trokhanyak, V.I., 2015. Computer mathematical modelling of heat and mass transfer of air ventilation in poultry houses. In: Bulletin of the Russian Scientific and Research Institute of Electrification of Agriculture, vol. 4(20), pp. 85-90.
8. Gorobets, V.G., Trokhanyak, V.I., Bogdan, Yu.O., 2015. Experimental study of cooling air supply poultry premises. In: Scientific Bulletin of National University of Life and Environmental Sciences of Ukraine. "Technologies and Power Engineering", vol. 224, pp. 204-208.
9. Gyl, L.S., Pashkovskiy, A.I., Sulima, L.T., 2008. Modern Technology of Protected and Open Horticulture. Part 1. Under Cover. Textbook. Publishing in Vinnytsa, Ukraine: "Nova Knyha", 368 p.
10. Korobiichuk, I., Lysenko, V., Reshetiuk, V. et al., 2016. Energy-efficient electrotechnical complex of greenhouses with regard to quality of vegetable production. In: International Conference on Systems, Control and Information Technologies, vol. 543, pp. 243-251.
11. Lateş, M.T., 2008. The Finite Element Method: Applications [in Romanian]. Transilvania University Publishing House Brasov, Romania.
12. Lysenko, V.P., Lendel, T.I., 2015. Optimal Control Strategy Models for Managing Areas Under Cover. In Bulletin of Agrarian Science, vol. 10, pp. 45-48.
13. Lysenko, V., Miroshnyk, V., Lendiel, T., 2015. Modeling the spatial distribution of temperature zones in the greenhouse. In: Bulletin of Agrarian Science, vol. 7(1-2), pp. 159-164.
14. Modest, M.F., 2013. Radiative Heat Transfer (Third Edition). Publishing in: Academic Press, 897 p.

15. Murthy, J.Y., Mathur, S.R., 1998. Finite volume method for radiative heat transfer using unstructured meshes. In: *Journal of Thermophysics and Heat Transfer*, vol. 12(3), pp. 313-321.
16. Raithby, G.D., Chui, E.H., 1990. Finite-volume method for predicting a radiant heat transfer in enclosures with participating media. In: *Journal of Heat Transfer*, vol. 112(2), pp. 415-423.
17. Shlyhtyng, H., 1974. Boundary layer theory. By publishing in: "Science", Moskov, Russia, 713 p.
18. Spalart, P., Allmaras, S., 1992. A one-equation turbulence model for aerodynamic flows. In: 30th Aerospace Sciences Meeting and Exhibit, Aerospace Sciences Meetings.
19. Spalart, P.R., Allmaras, S.R., 1994. A One-Equation Turbulence Model for Aerodynamic Flows. In: *La Recherche Aérospatiale*, no. 1, pp. 5-21.
20. Trokhanyak, V.I., Bogdan, Yu.O., 2015. The finite element method in making up meshes in ANSYS Meshing for CFD models. In: *Bulletin of Pryazovslyi State Technical University*, vol. 30(2), pp. 181-189.